Synthesis, Characterization, and Electrochemical Application of $Ca(OH)_2$-, $Co(OH)_2$-, and $Y(OH)_3$-Coated $Ni(OH)_2$ Tubes

Weiyang Li, Shaoyan Zhang, and Jun Chen*

Institute of New Energy Materials Chemistry, Nankai University, Tianjin 300071, P. R. China

Received: April 14, 2005

We report on the synthesis, characterization, and electrochemical application of $Ca(OH)_2$-, $Co(OH)_2$-, and $Y(OH)_3$-coated $Ni(OH)_2$ tubes with mesoscale dimensions. These composite tubes were prepared via a two-step chemical precipitation within an anodic alumina membrane under ambient conditions. The morphology and structure of the as-synthesized samples were characterized by X-ray diffraction (XRD), scanning electron microscopy (SEM), transmission electron microscopy (TEM), and high-resolution transmission electron microscopy (HRTEM) equipped with energy dispersive spectroscopy (EDS). The results showed that the size of the tubes was of mesoscale dimension and the proportion of the tube morphology was about 95%. The as-prepared composite tubes were further investigated as the positive-electrode materials of rechargeable alkaline batteries. Electrochemical measurements revealed that the $Ni(OH)_2$ tubes coated with $Ca(OH)_2$, $Co(OH)_2$, and $Y(OH)_3$ exhibited superior electrode properties including high discharge capacity, excellent high-temperature and high-rate discharge ability, and good cycling reversibility. The mechanism analysis suggests that both the coated layers and the unique hollow-tube structures play an indispensable role in optimizing the electrochemical performance of nickel hydroxide electrodes.

Introduction

Over the past few years, rechargeable batteries have become key components of portable, entertainment, computing, and telecommunication equipment required by today's information-rich and mobile society.[1−3] Nickel hydroxide is widely used as the active material for positive electrodes in Ni-based alkaline rechargeable batteries including nickel/cadmium (Ni/Cd), nickel/iron (Ni/Fe), nickel/metal hydride (Ni/MH), and nickel/zinc (Ni/Zn).[4,5] The high power density, good cycling ability, and relatively low cost of nickel electrodes have made these batteries very competitive for an extended range of applications. It is known that the capacities of the Ni-based alkaline rechargeable batteries are usually positive-electrode limited for reasons of proper recombination reactions and battery safety, and thus, it is of great scientific and technological importance to improve the properties of the nickel hydroxide electrode so as to enhance the performance of such batteries.

To improve the characteristics of the nickel hydroxide electrode, considerable efforts have been made in researching spherical $Ni(OH)_2$ powder with various additives such as cobalt, calcium, zinc, or rare-earth-based oxides and hydroxides, related composite materials, and technologies for battery production.[6−12] The addition of the calcium compound has an effect on the oxygen evolution potential of the nickel electrode.[8,9] Rare-earth-based additives show great influence on the high-temperature performance of the batteries.[10] Advanced cobalt additives beneficially improve the utilization and conductivity of the active materials.[11] It has also been reported that nickel hydroxide particles with a small crystalline size exhibit better electrochemical properties.[13] On one hand, spherical nickel hydroxide powder, which suppresses the development of inner-pore volume, makes it possible to increase the density of the active material itself. On the other hand, the core of spherical nickel hydroxide powder is still inactive, especially at high-rate or high-temperature charge/discharge due to the diffusion barrier.

In recent years, with the rapid development of one-dimensional (1D) nanostructures, the synthesis of 1D-nanostructure electrode materials, especially nanotubes, has attracted intense attention and shown great promise for boosting the performance of rechargeable batteries.[14] For the formation of nanotubes, it has been demonstrated that graphite and inorganic materials with similar layered structures can be turned into tubular structures by the rolling process.[15] Meanwhile, the simplest route to nanotubes is probably the template synthesis using nanoporous membranes with ordered and vertical 1D-channel structures.[16] By using the template method, not only layered structural materials[17] but also other various kinds of materials, such as metals,[18] semiconductors,[19] and polymers,[20] can be prepared into 1D nanostructures.

Up to now, nickel hydroxide nanostructures with different morphologies have been prepared. Zhu's group[21] synthesized $Ni(OH)_2$ nanosheets with hexagonal structure via a hydrothermal approach. Matsui et al.[22] prepared single-crystal $Ni(OH)_2$ nanorods by a hydrothermal method within carbon-coated alumina films. Liu and co-workers[23] synthesized $Ni(OH)_{1.66}(SO_4)_{0.17}(H_2O)_{0.29}$ nanoribbons through the treatment of freshly precipitated nickel hydroxide with high concentrations of nickel sulfate. By far, only a few studies have been focused on the fabrication of 1D nickel hydroxide nanostructures, and the investigation of their electrochemical activity was also limited. In addition, very little research has been done with respect to nickel hydroxide nanotubes. Recently, our group[24] synthesized mesoscale $Ni(OH)_2$ tubes via a template method and found that $Ni(OH)_2$ tubes, which allow diffusion and oxidation/reduction to occur easily, exhibit superior electrochemical properties such as high capacity and good cycling reversibility. Since $Ni(OH)_2$ tubes display meaningful advantages as positive-electrode materials for alkaline rechargeable batteries and, furthermore, since the utilization of the active materials at high-temperature

* Corresponding author. Fax: +86-22-2350-9118. E-mail: chenabc@nankai.edu.cn.

10.1021/jp051948o CCC: $30.25
Published on Web 07/06/2005

and high-rate charge/discharge is very critical for high-power output applications, such as electric and hybrid vehicles, investigation of composite $Ni(OH)_2$ tubes should be of great interest from both fundamental and applied perspectives.

Herein, we report on the template synthesis of $Ca(OH)_2$-, $Co(OH)_2$-, and $Y(OH)_3$-coated $Ni(OH)_2$ tubes via a two-step precipitation within porous alumina membranes. The electrochemical performance of the as-prepared tubes as positive-electrode materials for alkaline rechargeable batteries was systematically investigated by cyclic voltammetry and a galvanostatic method. The results show that the composite $Ni(OH)_2$ tubes are promising positive-candidates in the field of alkaline rechargeable batteries.

Experimental Section

Sample Preparation and Characterization. Anodic aluminum oxide membranes (Whatman, Φ47 mm with 0.2-μm pores and a 60-μm thickness) were used as the templates. $Ni(NO_3)_2 \cdot 6H_2O$, $CaCl_2 \cdot 2H_2O$, $Co(NO_3)_2 \cdot 6H_2O$, $Y(NO_3)_3 \cdot 6H_2O$, ammonia, and other reagents were all of analytical grade and used without further purification. Spherical β-$Ni(OH)_2$ particles coated with 5 wt % $Co(OH)_2$ were purchased from the Tanaka Chemical Corporation (Japan).

The $Ni(OH)_2$ tubes coated with 5 wt % $Ca(OH)_2$, $Co(OH)_2$, or $Y(OH)_3$ were synthesized via a chemical deposition method within the alumina membranes by using the following procedures: (1) The alumina templates were gently immersed in a 0.1 M $CaCl_2 \cdot 2H_2O$, $Co(NO_3)_2 \cdot 6H_2O$, or $Y(NO_3)_3 \cdot 6H_2O$ aqueous solution for 1 h so that the solution can be fully impregnated in the pore walls of the membranes. (2) Excess solution on the membrane surface was wiped off carefully by polishing with laboratory tissue. (3) 0.5 M ammonia was slowly dripped onto the membranes so that the ammonia solution gradually penetrated the templates under gravity and an adhesive driving force to react with $CaCl_2$, $Co(NO_3)_2$, or $Y(NO_3)_3$. (4) A similar procedure was carried out for the precipitation of $Ni(OH)_2$ inside the formed layer of $Ca(OH)_2$, $Co(OH)_2$, or $Y(OH)_3$ within the porous template except that, in this procedure, the reaction time was longer and the solution concentration was higher. (5) To obtain self-sustained nanotubes, the alumina membranes were dissolved in 2 M NaOH for 3 h. The remaining solid was collected, then rinsed with deionized water and absolute ethanol several times, and, finally, dried at 60 °C in a vacuum for 2 h.

For comparison, pure $Ni(OH)_2$ tubes were also prepared without the precipitation of the coated layer. The chemical reactions involved in the preparation process can be expressed as

Nanotube Preparation:

$$CaCl_2 \cdot 2H_2O + 2NH_4OH \rightarrow Ca(OH)_2\downarrow + 2NH_4Cl + 2H_2O \quad (1)$$

$$Co(NO_3)_2 \cdot 6H_2O + 2NH_4OH \rightarrow Co(OH)_2\downarrow + 2NH_4NO_3 + 6H_2O \quad (2)$$

$$Y(NO_3)_3 \cdot 6H_2O + 3NH_4OH \rightarrow Y(OH)_3\downarrow + 3NH_4NO_3 + 6H_2O \quad (3)$$

$$Ni(NO_3)_2 \cdot 6H_2O + 2NH_4OH \rightarrow Ni(OH)_2\downarrow + 2NH_4NO_3 + 6H_2O \quad (4)$$

Template dissolution:

$$Al_2O_3 + 2NaOH \rightarrow 2NaAlO_2 + H_2O \quad (5)$$

The phase structure of the as-prepared samples was analyzed using a Rigaku INT-2000 X-ray diffractometer (XRD) with Cu Kα radiation. Surface images were characterized with a Philips XL-30 scanning electron microscope (SEM). The transmission electron microscopy (TEM) and high-resolution transmission electron microscopy (HRTEM) images were taken on a Philips Tecnai-F20 transmission electron microscope using an accelerating voltage of 200 kV equipped with an energy dispersive spectrometer.

Electrochemical Measurements. Nickel hydroxide electrodes were prepared by inserting an active paste into a nickel foam substrate. A paste containing 85 wt % active materials (5 wt % $Co(OH)_2$-coated nickel hydroxide spherical powder, or pure $Ni(OH)_2$ tubes, or $Ni(OH)_2$ tubes coated with 5 wt % $Ca(OH)_2$, $Co(OH)_2$, or $Y(OH)_3$), 10 wt % carbon black, and 5 wt % poly(tetrafluoroethylene) (PTFE) was used. The electrode was dried at 80 °C for 1 h and cut into a disk (1.2×1.2 cm^2), which was pressed at a pressure of 100 kg cm^{-2} to a thickness of 0.4 mm. Then the electrode was spot-welded to a nickel sheet for electrical connection. Electrochemical performance of the electrodes was measured with a Solartron SI 1260 potentionstat analyzer with 1287 Interface and an Arbin charge/discharge unit at controlled temperatures in an electrochemical cell, which contained the nickel hydroxide working electrode, a metal hydride electrode, a Hg/HgO reference electrode, and a 6 M KOH solution as the electrolyte. The discharge capacity of the nickel hydroxide in the positive electrode was based on the amount of active material $Ni(OH)_2$ without taking into account the additives in the electrode. The discharge capacity of each electrode was expressed in milliampere hours per gram of the active material.

Results and Discussion

Figure 1a shows the XRD pattern of the 5 wt % $Co(OH)_2$-coated β-$Ni(OH)_2$ spheres purchased. All the peaks can be indexed as a single phase of well-crystallized β-$Ni(OH)_2$ with the hexagonal structure (ICDD-JCPDS card No. 14-0117). No peaks due to pure $Co(OH)_2$ or others were observed, indicating that the additives have no influence on the crystal structure of the powders. This may be due to the Co^{2+} replacement with Ni^{2+} in the lattice or the amorphous state of $Co(OH)_2$. Figure 1b−d show the SEM images of the 5 wt % $Co(OH)_2$-coated β-$Ni(OH)_2$ spheres at different magnifications. At low magnification (Figure 1b), the sample consists of quasi-spherical particles with an average particle size of about 15 μm. At relatively high magnifications (Figure 1c and d), the particles are made up of agglomerations with small needles and flakes to form quasi-spherical particles.

Figure 2 shows the XRD patterns of the four as-synthesized $Ni(OH)_2$ tubes. Figure 2A is the XRD pattern of the pure $Ni(OH)_2$ tubes, while B, C, and D are the XRD patterns of the $Ni(OH)_2$ tubes coated with 5 wt % $Ca(OH)_2$, $Co(OH)_2$, and $Y(OH)_3$, respectively. It can be observed that the position of the characteristic peaks of B, C, and D is the same as that of A. All the diffraction peaks can be readily indexed to the β-$Ni(OH)_2$ with the hexagonal structure (ICDD-JCPDS card No. 14-0117). No peaks from other phases were observed, indicating that the amounts of the additives ($Ca(OH)_2$, $Co(OH)_2$, and $Y(OH)_3$) are very small and have no influence on the crystal structure.

Figure 3 shows the SEM images of the as-prepared β-$Ni(OH)_2$ tubes: without any additive (Figure 3A) and coated with 5 wt % $Ca(OH)_2$ (Figure 3B), $Co(OH)_2$ (Figure 3C), and $Y(OH)_3$ (Figure 3D). It can be observed that the as-prepared tubes are

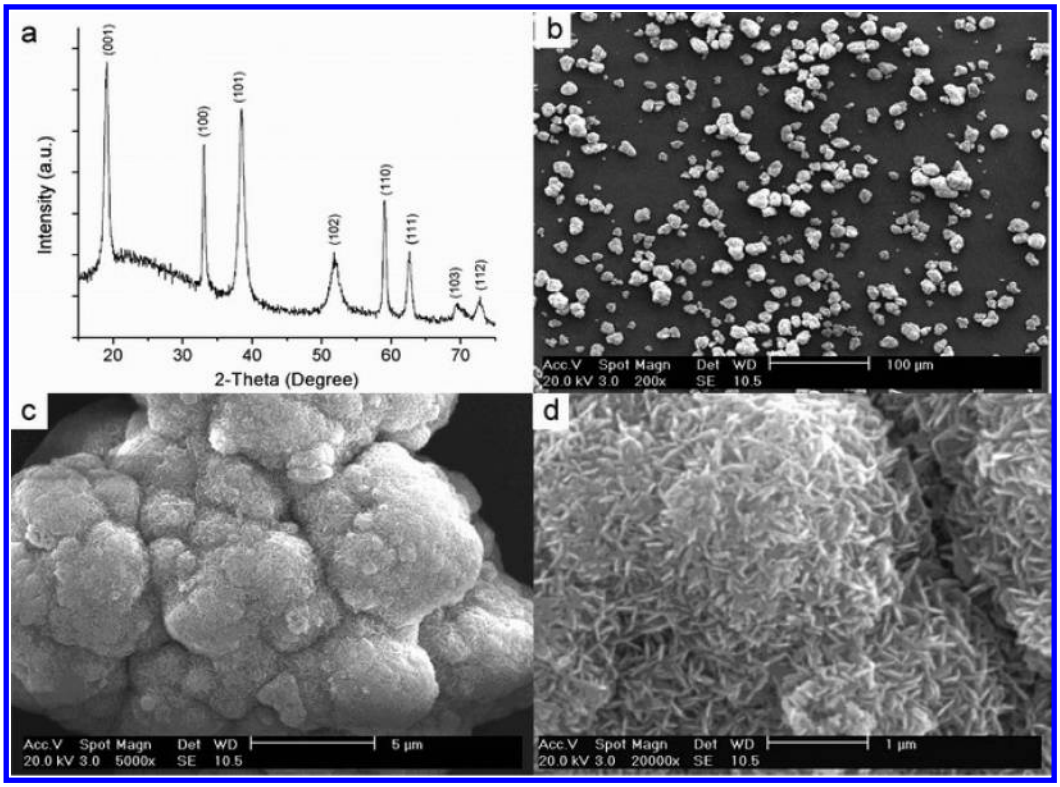

Figure 1. XRD pattern (a) and SEM images at low magnification (b) and relatively high magnifications (c and d) of the spherical β-$Ni(OH)_2$ particles coated by 5 wt % $Co(OH)_2$.

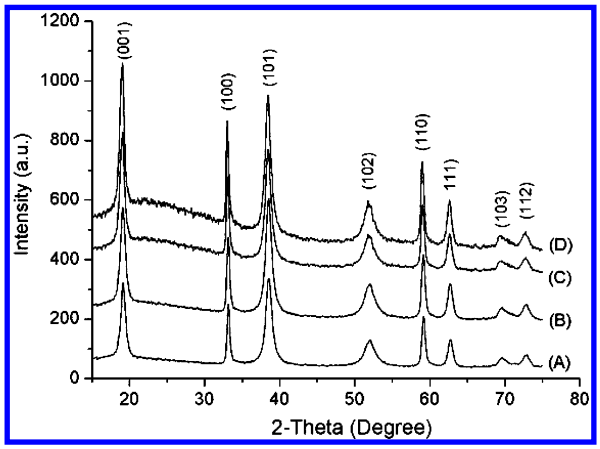

Figure 2. XRD patterns of the as-prepared β-$Ni(OH)_2$ tubes: (A) without any additive and (B−D) coated with 5 wt % (B) $Ca(OH)_2$, (C) $Co(OH)_2$, and (D) $Y(OH)_3$.

hollow inside and the average outer diameters are approximately 200 nm, well consistent with the pore diameters of the template membrane used in the synthesis process. The length of the tubes is smaller than the thickness of the template, suggesting that long tubes are broken into shorter ones. This may be due to the process of template dissolution and drying, which indicates limited mechanical strength of the tubes. The surfaces of the tubes in Figure 3B, C, and D are rougher than those of the tubes in Figure 3A, owing to the coated layer of $Ca(OH)_2$, $Co(OH)_2$, or $Y(OH)_3$.

Further insight into the morphology and microstructure of the as-prepared tubes was investigated by TEM (Figure 4). Figure 4A-1 shows the TEM image of a group of pure $Ni(OH)_2$ tubes scattered on the copper mesh, while Figure 4B-1, C-1, and D-1 are the images of groups of $Ca(OH)_2$-, $Co(OH)_2$-, and $Y(OH)_3$-coated $Ni(OH)_2$ tubes, respectively. The central parts of these mesostructures are brighter in contrast to their edges, confirming their hollow-tube nature. The average outer diameter of the walls surrounding the central hollow core is approximately 200 nm, consistent with that observed in the SEM images of Figure 3. It is noticed that the wall thickness of the tubes in Figure 4B-2, C-2, and D-2 is about 50−70 nm, much thicker than that of the tube in Figure 4A-2 (about 20−30 nm), illustrating the formation of the coated layers. On the basis of the observations of SEM and TEM, the proportion of the tube morphology was estimated to be about 95%. Therefore, the size of the tubes is definitely of mesoscale dimension under our synthesis conditions. The chemical compositions of these tubes were analyzed by energy-dispersive spectroscopy (EDS). Figure 4A-3 shows the EDS pattern of the pure $Ni(OH)_2$ tubes: the peaks of Ni and O demonstrated the existence of $Ni(OH)_2$; the peaks of Cu and C came from the copper mesh and carbon film that supported the sample in the TEM analysis; the presence of Al was due to the remaining trace of the alumina matrix. Meanwhile, the EDS patterns of the tubes coated with $Ca(OH)_2$ (Figure 4B-3), $Co(OH)_2$ (Figure 4C-3), and $Y(OH)_3$ (Figure 4D-3) are similar to that of the pure $Ni(OH)_2$ tubes, although the peaks of Ca, Co, and Y were detected due to the coating of $Ca(OH)_2$, $Co(OH)_2$, and $Y(OH)_3$, respectively. On the basis of the EDS analysis, the calculated weight ratio of $Ni(OH)_2$ and the coated layers ($Ca(OH)_2$, $Co(OH)_2$, or $Y(OH)_3$) is approximately 95:5. Figure 5 shows the HRTEM image of the wall of the $Co(OH)_2$-coated $Ni(OH)_2$ tube. It can be observed that the wall is composed of an array of continuous, ultrafine, multilayered nanoparticles. The HRTEM analyses of the other as-synthesized coated tubes are similar to that of Figure 5, also showing the composition of ultrafine nanoparticles.

Figures 6 and 7 show the cyclic voltammograms (CVs) of the spherical 5 wt % $Co(OH)_2$-coated $Ni(OH)_2$ electrode and the as-prepared tube electrodes in the first cycle, respectively. Similarly shaped voltammograms were also obtained for five-

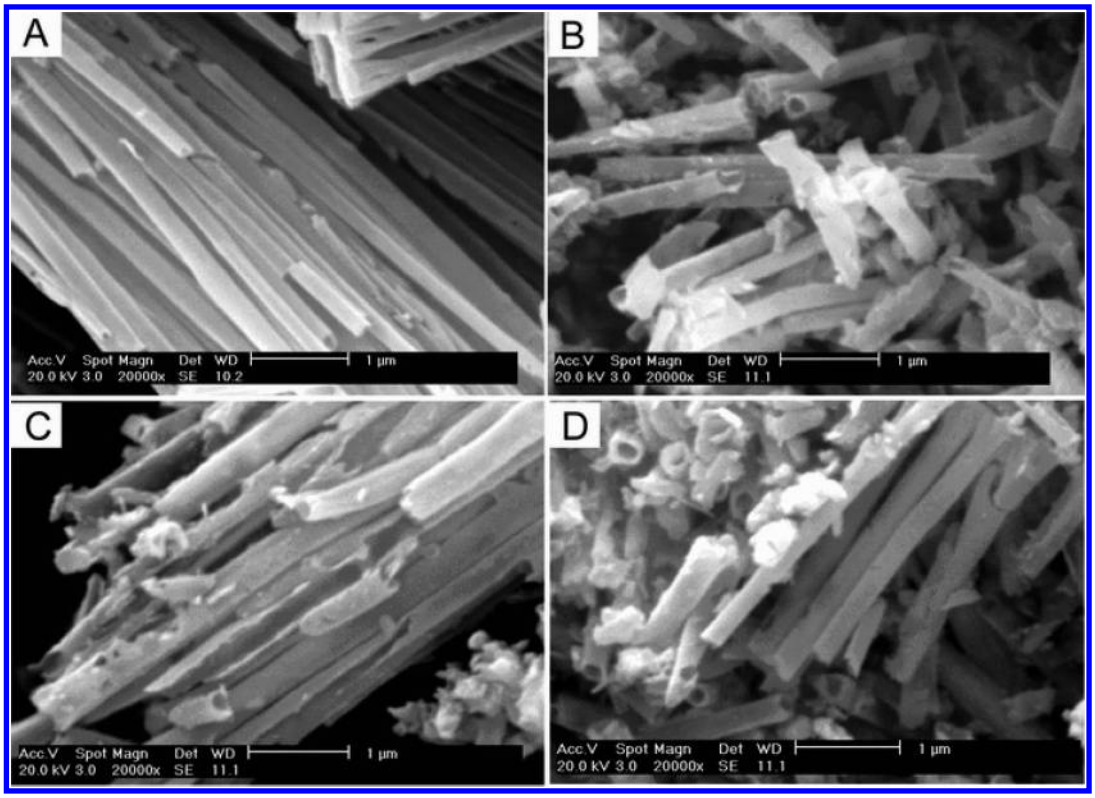

Figure 3. SEM images of the as-prepared β-$Ni(OH)_2$ tubes: (A) without any additive and (B−D) coated with 5 wt % (B) $Ca(OH)_2$, (C) $Co(OH)_2$, and (D) $Y(OH)_3$.

potential cycling. Reversible peaks are observed for the spherical-particle and tube electrodes, but their characteristics are different. The features of the voltammograms are summarized in Table 1. The main interpretation follows. First, when the electrodes were scanned cathodically, two peaks, for the oxidation potential, E_O, and oxygen-evolution potential, E_{OE}, appeared; during the following anodic polarization, only one peak was observed, which was assigned to the reduction potential, E_R. Second, the difference between the oxidation potential and the reduction potential, $E_O - E_R$, is taken as a measure of the reversibility of the electrode reaction. The smaller this value, the more reversible is the electrode reaction. Third, the difference between the oxygen-evolution potential and the oxidation potential, $E_{OE} - E_O$, is also an important parameter for judging the performance of the nickel electrode. This value indicates the charge efficiency of the electrode. The bigger this value is, the more fully the electrode can be charged before oxygen evolution, namely, the higher the utilization of active material (more complete oxidation of Ni^{2+} to Ni^{3+}).

TABLE 1: Reduction Potential, E_R, Oxidation Potential, E_O, Oxygen-Evolution Potential, E_{OE}, $E_O - E_R$, and $E_{OE} - E_O$ for the Spherical 5 wt % $Co(OH)_2$-Coated $Ni(OH)_2$ Particle Electrode and the As-Prepared Pure and Coated $Ni(OH)_2$ Tube Electrodes at 20 °C

electrode	potentials (mV)				
	E_R	E_O	E_{OE}	$E_O - E_R$	$E_{OE} - E_O$
spherical $Ni(OH)_2$	335	512	559	176	47
pure $Ni(OH)_2$ tube	365	497	562	132	65
$Ni(OH)_2/Ca(OH)_2$ tube	380	490	562	110	72
$Ni(OH)_2/Co(OH)_2$ tube	390	480	562	90	82
$Ni(OH)_2/Y(OH)_3$ tube	401	470	562	69	92

From Table 1, it can also be seen that the spherical $Ni(OH)_2$ powder electrode shows the biggest value of $E_O - E_R$ and the smallest value of $E_{OE} - E_O$, illustrating that the reaction reversibility of electrodes made of the tubes is much better than that of the spherical particle. In particular, by coating the tubes with $Ca(OH)_2$, $Co(OH)_2$, and $Y(OH)_3$, the reaction reversibility has been greatly improved, especially for the electrode made of tubes coated with 5 wt % $Y(OH)_3$ (according to its smallest value of $E_O - E_R$ and biggest value of $E_{OE} - E_O$). Consequently, it demonstrates that the tube electrodes present electrochemical-cyclic properties superior to those of the spherical particle electrode. Because the spherical 5 wt % $Co(OH)_2$-coated $Ni(OH)_2$ particle electrode showed the poorest reaction reversibility, further electrochemical measurements were not carried out on this electrode.

Figure 8 shows the discharge curves of the as-prepared β-$Ni(OH)_2$ tube electrodes in the fifth cycle at the current density of 50 mA g^{-1} and 20 °C. It can be observed that the discharge capacity of the $Ni(OH)_2$ tube electrodes coated with $Ca(OH)_2$, $Co(OH)_2$, and $Y(OH)_3$ is 277 mA h g^{-1}, 289 mA h g^{-1}, and 282 mA h g^{-1}, respectively, which is lower than that of the pure $Ni(OH)_2$ tube electrode (315 mA h g^{-1}). However, the coated tube electrodes display a higher discharge plateau potential and a more steady discharge plateau.

Figure 9 shows the relationship between the working temperature and the discharge capacity of the pure and coated $Ni(OH)_2$ tube electrodes. In practical application, nickel electrodes should have a stable discharge capacity in a wide temperature range. It can be seen that the discharge capacity of all the electrodes decreased with increasing working temperature. Obviously, the capacity of the pure tube electrode decreased much more quickly than that of the coated tube electrodes. At 60 °C, the $Ni(OH)_2$ tube electrodes coated with $Ca(OH)_2$, $Co(OH)_2$, and $Y(OH)_3$ still retained 252 mA h g^{-1}, 267 mA h g^{-1}, and 259 mA h g^{-1}, corresponding to 91.0%, 92.4%, and 91.8% of their capacities at 20 °C, respectively, while the pure tube electrode only showed a retention of about 79.7% of its capacity at 20 °C.

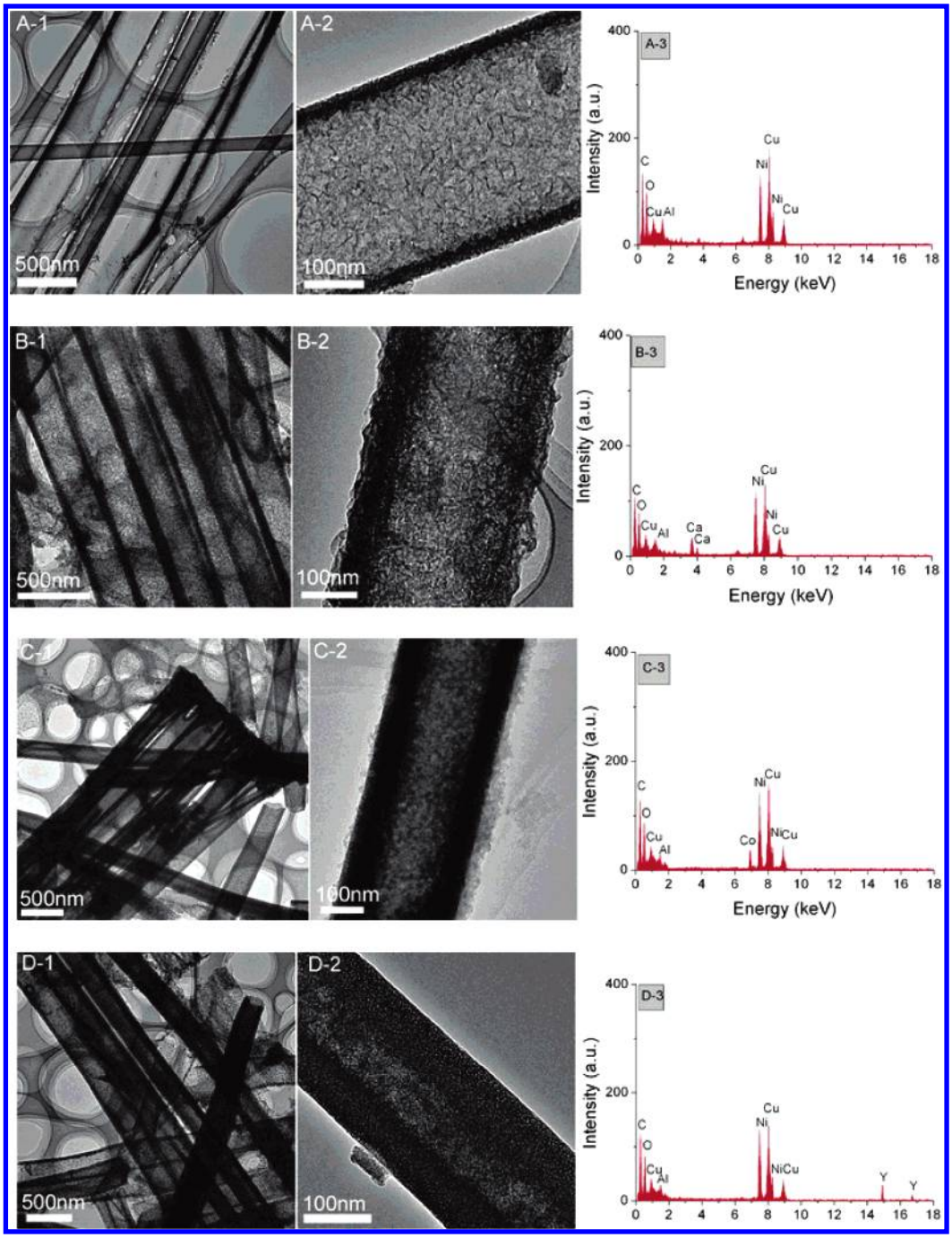

Figure 4. TEM images (A-1, A-2, B-1, B-2, C-1, C-2, D-1, and D-2) and EDS analyses (A-3, B-3, C-3, and D-3) of the as-prepared β-$Ni(OH)_2$ tubes: (A) without any additive and (B−D) coated with 5 wt % (B) $Ca(OH)_2$, (C) $Co(OH)_2$, and (D) $Y(OH)_3$.

Figure 10 presents the effect of discharge current density on the electrode capacity. The capacity of each electrode decreased with increasing discharge current density. At 300 mA g^{-1}, the $Ni(OH)_2$ tube electrodes coated with $Ca(OH)_2$, $Co(OH)_2$, and $Y(OH)_3$ still retained 190 mA h g^{-1}, 209 mA h g^{-1}, and 202 mA h g^{-1}, corresponding to 68.6%, 72.3%, and 71.7% of their capacities at 50 mA g^{-1}, respectively, while the pure tube electrode only showed 180 mA h g^{-1} (about 57% of its capacity at 50 mA g^{-1}). As shown in Figures 9 and 10, it is obvious that the high-temperature and high-rate discharge abilities of the nickel hydroxide electrode, which is critical for alkaline rechargeable batteries for high-power output, have been significantly improved by $Ca(OH)_2$, $Co(OH)_2$, or $Y(OH)_3$ coating. The sequence of their high-temperature and high-rate discharge ability from best to worst is $Ni(OH)_2/Co(OH)_2$ tube > $Ni(OH)_2/Y(OH)_3$ tube > $Ni(OH)_2/Ca(OH)_2$ tube > pure $Ni(OH)_2$ tube.

Figure 11 shows the curves of discharge capacity vs cycle number for the electrodes made by pure and coated $Ni(OH)_2$ tubes at the current density 50 mA g^{-1} and 20 °C. Starting from the fifth cycle, the discharge capacity decreased with increasing cycle numbers. After 100 cycles with 100% depth of charge and discharge, the $Ni(OH)_2$ tube electrodes coated with $Ca(OH)_2$, $Co(OH)_2$, and $Y(OH)_3$ retained 267 mA h g^{-1}, 281 mA h g^{-1}, and 276 mA h g^{-1}, corresponding to 96.4%, 97.3%, and 97.9% of their capacity in the fifth cycle, respectively, while the pure tube electrode showed a retention of about 95.5% of its capacity in the fifth cycle. That is, the average capacity fading per cycle of the $Ca(OH)_2$-, $Co(OH)_2$-, and $Y(OH)_3$-coated tube

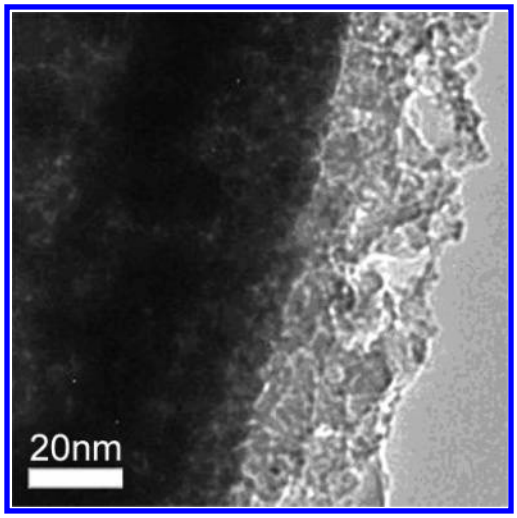

Figure 5. HRTEM image of the outside wall of the as-synthesized $Co(OH)_2$-coated $Ni(OH)_2$ tube.

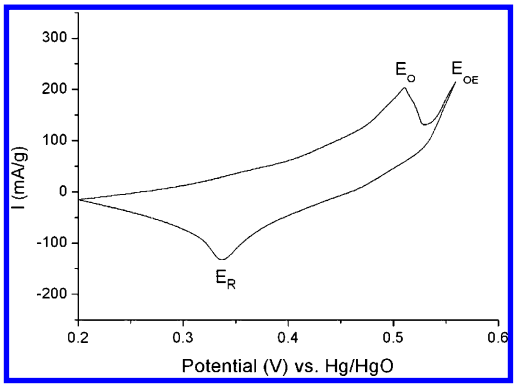

Figure 6. Cyclic voltammogram of the electrode made by 5 wt % $Co(OH)_2$-coated $Ni(OH)_2$ spheres at a scan rate of 0.5 mV/s and 20 °C.

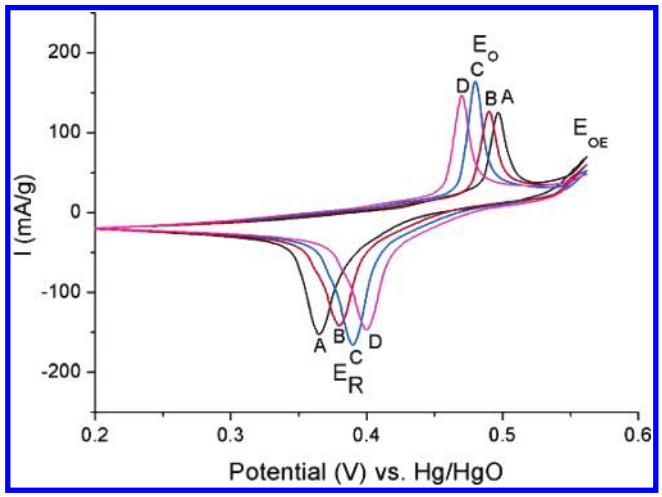

Figure 7. Cyclic voltammograms of the electrodes made by the as-prepared β-$Ni(OH)_2$ tubes: (A) without any additive and (B−D) coated with 5 wt % (B) $Ca(OH)_2$, (C) $Co(OH)_2$, and (D) $Y(OH)_3$ at a scan rate of 0.5 mV/s and 20 °C.

electrodes is about 0.105 mA h g^{-1}, 0.084 mA h g^{-1}, and 0.063 mA h g^{-1}, respectively, while that of the pure tube electrode is 0.158 mA h g^{-1}. This indicates that the rate of capacity decay displays the following order: pure $Ni(OH)_2$ tube > $Ni(OH)_2$/$Ca(OH)_2$ tube > $Ni(OH)_2$/$Co(OH)_2$ tube > $Ni(OH)_2$/$Y(OH)_3$ tube. It is noted that the cycling performance of the $Ni(OH)_2$ tube electrodes is enhanced by the coated layers, although the

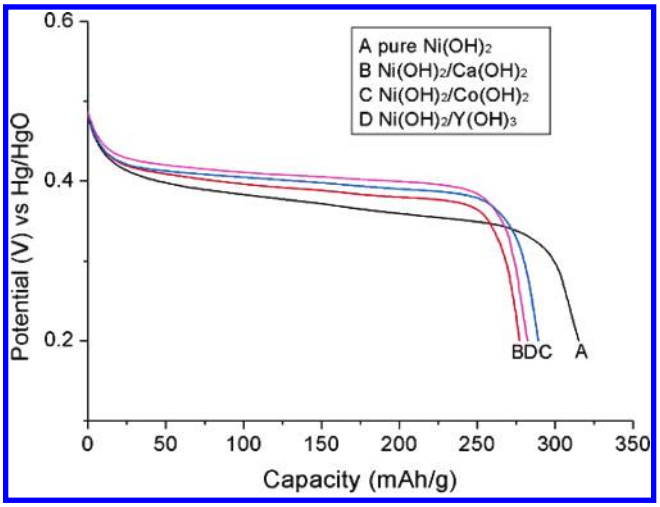

Figure 8. Discharge curves as a function of capacity for electrodes made by the as-prepared $Ni(OH)_2$ tubes: (A) without any additive and (B−D) coated with 5 wt % (B) $Ca(OH)_2$, (C) $Co(OH)_2$, and (D) $Y(OH)_3$ at the current density of 50 mA g^{-1} and 20 °C.

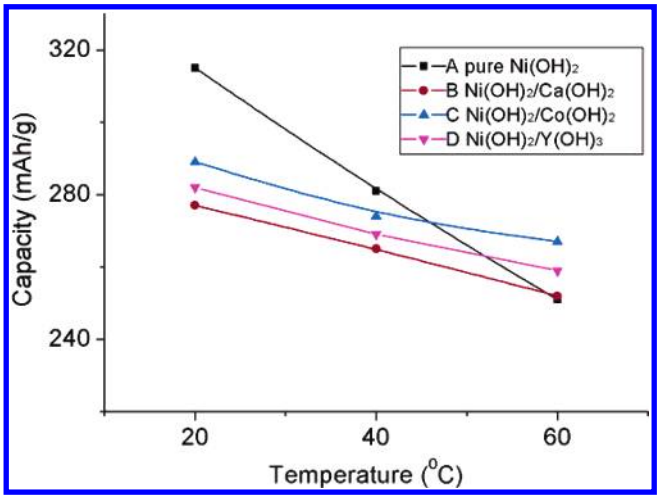

Figure 9. Discharge capacity of the electrodes made by the as-prepared $Ni(OH)_2$ tubes: (A) without any additive and (B−D) coated with 5 wt % (B) $Ca(OH)_2$, (C) $Co(OH)_2$, and (D) $Y(OH)_3$ vs different working temperatures at the current density of 50 mA g^{-1}.

capacity of the coated tube electrodes is a little lower than that of the pure tube electrode. This indicates excellent reaction reversibility of the composite tube electrodes, especially the $Y(OH)_3$-coated tube electrode, which is consistent with the results obtained in the CVs.

According to the results presented above, both pure and coated $Ni(OH)_2$ tube electrodes exhibited electrochemical properties superior to those of the spherical $Ni(OH)_2$ powder electrode: the pure $Ni(OH)_2$ tube electrode displayed the highest discharge capacity at relatively low temperatures and a low discharge current density, whereas the coated $Ni(OH)_2$ tube electrodes displayed excellent high-temperature and high-rate electrochemical performance and better capacity retention, showing significant potential for applications in high power fields such as electric vehicles. This may be explained as follows.

First, it is known that the reversible nickel electrode reaction may be briefly described by the equation

$$\beta\text{-}Ni(OH)_2 + OH^- \rightleftharpoons \beta\text{-}NiOOH + H_2O + e^- \qquad (6)$$

Traditionally, the theoretical capacity of the nickel hydroxide

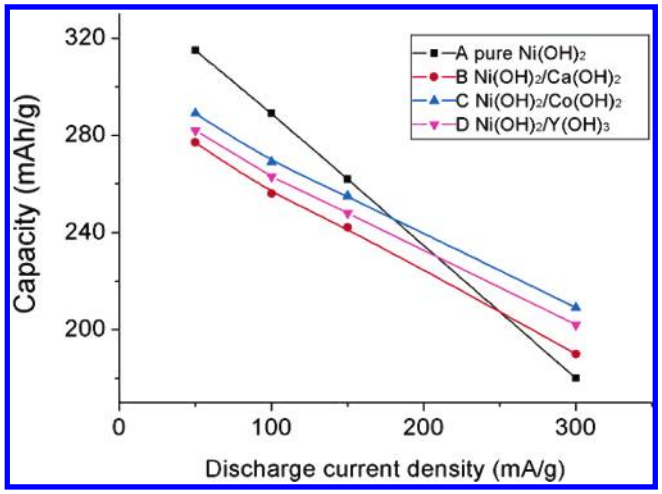

Figure 10. Discharge capacity of the electrodes made by the as-prepared $Ni(OH)_2$ tubes: (A) without any additive and (B−D) coated with 5 wt % (B) $Ca(OH)_2$, (C) $Co(OH)_2$, and (D) $Y(OH)_3$ vs different discharge current densities at 20 °C.

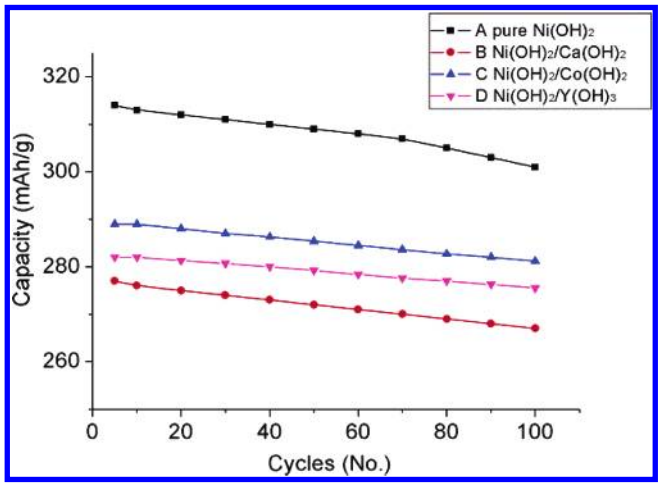

Figure 11. Cycle life of the electrodes made by the as-prepared Ni-$(OH)_2$ tubes: (A) without any additive and (B−D) coated with 5 wt % (B) $Ca(OH)_2$, (C) $Co(OH)_2$, and (D) $Y(OH)_3$ at the current density of 50 mA g^{-1} and 20 °C.

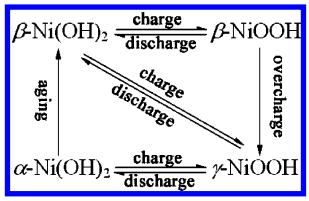

Figure 12. Phase transformation of the nickel hydroxide electrode during the charge/discharge process.

is believed to be 289 mA h g^{-1} if the electrode reaction involves one-electron transfer. However, the charge−discharge reactions, which actually take place in the nickel hydroxide electrode, are much more complex. It has been reported that four phases of nickel hydroxides and oxyhydroxides exist during the lifetime of a nickel hydroxide electrode, namely, β-$Ni(OH)_2$, β-NiOOH, γ-NiOOH, and α-$Ni(OH)_2$[25] (Figure 12).

The nickel oxidation state in γ-NiOOH is known to be 3.33 because of the Ni^{4+} defect,[26] and thus, the pure $Ni(OH)_2$ tube electrode yields a higher discharge capacity of 315 mA h g^{-1} at the current density of 50 mA g^{-1} and 20 °C, demonstrating that, in addition to the phase transformation of β-$Ni(OH)_2$ to β-NiOOH, partial formation of γ-NiOOH occurred. However, the formation of γ-NiOOH is associated with the volume expansion or swelling of the electrode, which interferes with effective contact between particles of active material, and this increases the resistance of the electrode reaction and leads to faster capacity decay, especially at high-rate or high-temperature charge/discharge.[27] On one hand, although the discharge capacities of the $Ni(OH)_2$-coated tube electrodes under general working conditions are a little lower ($Ni(OH)_2$/$Ca(OH)_2$, 277 mA h g^{-1}; $Ni(OH)_2$/$Co(OH)_2$, 289 mA h g^{-1}; $Ni(OH)_2$/$Y(OH)_3$, 282 mA h g^{-1}) compared with that of the pure $Ni(OH)_2$ tube electrode (315 mA h g^{-1}), they are close to the theoretical capacity of β-$Ni(OH)_2$ (289 mA h g^{-1}) and still much higher than that of the conventional spherical $Ni(OH)_2$ powder, as reported.[7−9] On the other hand, by coating the layer of $Ca(OH)_2$, $Co(OH)_2$, or $Y(OH)_3$ on $Ni(OH)_2$ tubes, the formation of γ-NiOOH can be suppressed, contributing to preventing the swelling of the electrode during numerous charge−discharge cycles and much higher utilization of the active material at high temperatures and a high discharge current density. Therefore, the composite tubes exhibit excellent high-rate and high-temperature discharge performance and better cycling stability.

Second, it is believed that the improvements to the electrochemical properties were related to enhancement of surface reactivity as the particle size decreased.[28] The as-synthesized composite tubes are composed of ultrafine nanoparticles and have large surface areas, helping to enhance the contact between the active material and the electrolyte. Meanwhile, the hollow-inside tube structure makes the proton diffuse from both outer and inner sides of the tube walls, which can provide more active sites and facilitate the proton diffusion and redox reaction, while the proton diffusion can merely occur on the surface of the spherical particle due to the diffusion barrier. As is known, the proton diffusion is the rate-determining step in the nickel hydroxide electrode,[29] and thereby, the increase in the rate of proton diffusion results in the decrease of electrode polarization. In addition, the hollow structure may lighten the stress caused by volume change during the numerous charge−discharge cycles and suppress the degradation of the electrode.

Third, it is noticed that the $Co(OH)_2$-coated $Ni(OH)_2$ tube electrode shows the best high-temperature and high-rate discharge ability. This may be due to the oxidation of $Co(OH)_2$ to CoOOH on the nickel hydroxide surface during the charge process.[6] The formation of cobalt(III) oxyhydroxide (CoOOH) not only builds a good conductive network between the nickel hydroxide and the substrates, which improves the proton conductivity and decreases the resistance of the electrode reaction, but is also capable of increasing oxygen evolution overpotential,[30] which leads to higher charge efficiency. Owing to the high degree of disorder and defects on the surface of nanostructure materials,[31] the nanophase CoOOH which was formed during the charge process could have a superior surface activity so that it may readily capture oxygen species to form a nonstoichiometric $Co^{3+}_{1-x}Co^{4+}_xOOH_{1-x}$ phase[11] in the period of charge termination and depressed oxygen evolution. Furthermore, it can also be observed that the $Y(OH)_3$-coated Ni-$(OH)_2$ tube electrode displays better electrochemical reaction reversibility; however, the detailed working mechanism is still not quite clear and needs to be further investigated.

To take advantage of the above electrodes, made by modified $Ni(OH)_2$ tubes, in the practical application of alkaline rechargeable batteries, one may note that the template synthesis must be developed on a large scale. To reduce the high cost of alumina membranes and to satisfy the needs of modern industry, soft templates such as polymers and block copolymers were also employed.[32] Polysulfone (PSF), one kind of polymer

material known for its many sources, low cost, and excellent properties, has been widely investigated for the preparation of hollow fiber membranes.[33] Our group has recently developed an approach for synthesizing flat nanoporous membranes using PSF, poly(ethylene glycol) (PEG), and dimethylacetamide (DMAC). The technique of using the as-prepared nanoporous polysulfone membrane for large-scale production of $Ni(OH)_2$ tubes is still being optimized, and the preparation process is similar to the procedure for preparing $Ni(OH)_2$ tubes within an alumina template. It mainly involves the following: (1) impregnating nickel ions in the pore walls of the membrane; (2) dropping ammonia solution through the membrane to precipitate nickel hydroxide; and (3) dissolving the membrane in DMAC solution to obtain the tube bundles. Further studies on the large-scale applications of this system are currently underway.

Conclusions

$Ni(OH)_2$ tubes coated with 5 wt % $Ca(OH)_2$, $Co(OH)_2$, or $Y(OH)_3$ were successfully prepared by a chemical deposition method within the ordered, porous alumina template under ambient conditions. The electrochemical performance of the as-prepared composite $Ni(OH)_2$ tubes as the positive-electrode materials of rechargeable alkaline batteries was systematically investigated by cyclic voltammetry and a galvanostatic method. The results illustrate that both pure and coated $Ni(OH)_2$ tube electrodes exhibited electrochemical performance superior to that of a conventional spherical $Ni(OH)_2$ powder electrode. The pure $Ni(OH)_2$ tube electrode displayed the highest discharge capacity, 315 mA h g^{-1}, under general working conditions (relatively low temperatures and a low discharge current density), while the composite $Ni(OH)_2$ tube electrodes displayed excellent high-temperature and high-rate electrochemical performance and superior capacity retention, showing great promise for high-power output applications. Among the coated tubes, the $Co(OH)_2$-coated $Ni(OH)_2$ tube electrode showed the best high-temperature and high-rate discharge ability, and the $Y(OH)_3$-coated $Ni(OH)_2$ tube electrode displayed the best electrochemical cycling reversibility. Mechanism analysis reveals that the improved electrode performance arises from the effects of the unique hollow-inside tube character and the coated layers. To take advantage of $Ni(OH)_2$ tubes in the practical application of alkaline rechargeable batteries, further studies of the large-scale production of $Ni(OH)_2$ tubes are needed.

Acknowledgment. This work was supported by the National NSFC (20325102 and 90406001) and MOE-Key Project (104055).

References and Notes

(1) Ovshinsky, S. R.; Fetcenko, M. A.; Ross, J. *Science* **1993**, *260*, 176.

(2) Tarascon, J. M.; Armand, M. *Nature* **2001**, *414*, 359.

(3) Whittingham, M. S. *Chem. Rev.* **2004**, *104*, 4271.

(4) (a) Bard, A. J.; Parsons, R.; Jordan, J. *Standard Potentials in Aqueous Solution*, IUPAC; Marcel Dekker Inc.: New York, 1985. (b) Linden, D.; Reddy, T. B. *Handbook of Batteries*, 3rd ed.; McGraw-Hill Inc.: New York, 2002.

(5) Winter, M.; Brodd, R. J. *Chem. Rev.* **2004**, *104*, 4063.

(6) Oshitani, M.; Watada, M.; Tanaka, T.; Iida, T. In *Hydrogen and Metal Hydride Batteries*; Bennett, P. D., Sakai, T., Eds.; Electrochemical Society: Pennington, NJ, 1994; Vol. 94-27, p 303.

(7) Wang, X. Y.; Yan, J.; Yuan, H. T.; Zhou, Z.; Song, D. Y.; Zhang, Y. S.; Zhu, L. G. *J. Power Sources* **1998**, *72*, 221.

(8) Yuan, A. B.; Cheng, S. O.; Zhang, J. Q.; Cao, C. N. *J. Power Sources* **1998**, *76*, 36.

(9) Chen, J.; Bradhurst, D. H.; Dou, S. X.; Liu, H. K. *J. Electrochem. Soc.* **1999**, *146*, 3606.

(10) Oshitani, M.; Watada, M.; Shodai, K. *J. Electrochem. Soc.* **2001**, *148*, A67.

(11) (a) Pralong, V.; Delahaye-Vidal, A.; Beaudoin, B.; Leriche, J. B.; Tarascon, J. M. *J. Electrochem. Soc.* **2000**, *147*, 1306. (b) Hu, W. K.; Gao, X. P.; Geng, M. M.; Gong, Z. X.; Noréus, D. *J. Phys. Chem. B* **2005**, *109*, 5392.

(12) Hu, W. K.; Noréus, D. *Chem. Mater.* **2003**, *15*, 974.

(13) (a) Konstantinov, K.; Zhong, S.; Wang, C. Y.; Liu, H. K.; Dou, S. X. *J. Nanosci. Nanotechnol.* **2003**, *2*, 675. (b) Wang, X. Y.; Luo, H.; Parkhutik, P. V.; Millan, A. C.; Matveeva, E. *J. Power Sources* **2003**, *115*, 153.

(14) (a) Che, G. L.; Lakshmi, B. B.; Fisher, E. R.; Martin, C. R. *Nature* **1998**, *393*, 346. (b) Fischer, J. E. *Acc. Chem. Res.* **2002**, *35*, 1079. (c) Lee, J. Y.; An, K. H.; Heo, J. K.; Lee, Y. H. *J. Phys. Chem. B* **2003**, *107*, 8812. (d) Wang, Y.; Takahashi, K.; Shang, H.; Cao, G. *J. Phys. Chem. B* **2005**, *109*, 3085. (e) Li, X. L.; Li, Y. D. *J. Phys. Chem. B* **2004**, *108*, 13893.

(15) (a) Iijima, S. *Nature* **1991**, *354*, 56. (b) Tenne, R.; Mrgulis, L.; Genut, M.; Hodes, G. *Nature* **1992**, *360*, 444. (c) Feldman, Y.; Wasserman, E.; Srolovitz, D. J.; Tenne, R. *Science* **1995**, *267*, 222. (d) Chopra, N. G.; Luyken, R. J.; Cherrey, K.; Crespi, V. H.; Cohen, M. L.; Louie, S. G.; Zettl, A. *Science* **1995**, *269*, 966. (e) Li, Y. D.; Wang, J. W.; Deng, Z. X.; Wu, Y. Y.; Sun, X. M.; Yu, D. P.; Yang, P. D. *J. Am. Chem. Soc.* **2001**, *123*, 9904.

(16) (a) Wu, C. G.; Bein, T. *Science* **1994**, *266*, 1013. (b) Martin, C. R. *Science* **1994**, *266*, 1961. (c) Sui, Y. C.; Acosta, D. R.; Gonzalez-Leon, J. A.; Bermudez, A.; Feuchtwanger, J.; Cui, B. Z.; Flores, J. O.; Saniger, J. M. *J. Phys. Chem. B* **2001**, *105*, 1523. (d) Xu, Q.; Zhang, L.; Zhu, J. *J. Phys. Chem. B* **2003**, *107*, 8294. (e) Shi, K.; Chi, Y.; Yu, H.; Xin, B.; Fu, H. *J. Phys. Chem. B* **2005**, *109*, 2546.

(17) (a) Zelenski, C. M.; Dorhout, P. K. *J. Am. Chem. Soc.* **1998**, *120*, 734. (b) Tenne, R. *Angew. Chem., Int. Ed.* **2003**, *42*, 5124.

(18) (a) Mbindyo, J. K. N.; Mallouk, T. E.; Mattzela, J. B.; Kratochvilova, I.; Razavi, B.; Jackson, T. N.; Mayer. T. S. *J. Am. Chem. Soc.* **2002**, *124*, 4020. (b) Sun, Y.; Tao, Z.; Chen, J.; Herricks, T.; Xia, Y. *J. Am. Chem. Soc.* **2004**, *126*, 5940.

(19) Sone, E. D.; Zubarev, E. R.; Stupp, S. I. *Angew. Chem., Int. Ed.* **2002**, *41*, 1706.

(20) Steinhart, M.; Wendorff, J. H.; Greiner, A.; Wehrspohn, R. B.; Nielsch, K.; Schilling, J.; Choi, J.; Gösele. U. *Science* **2002**, *296*, 1997.

(21) Liang, Z. H.; Zhu, Y. J.; Hu, X. L. *J. Phys. Chem. B* **2004**, *108*, 3488.

(22) Matsui, K.; Kyotani, T.; Tomita, A. *Adv. Mater.* **2002**, *14*, 1216.

(23) Yang, D. N.; Wang, R. M.; Zhang, J.; Liu, Z. F. *J. Phys. Chem. B* **2004**, *108*, 7531.

(24) Cai, F. S.; Zhang, G. Y.; Chen, J.; Gou, X. L.; Liu, H. K.; Dou, S. X. *Angew. Chem., Int. Ed.* **2004**, *43*, 4212.

(25) Halpert, G. In *Nickel Hydroxide Electrodes*; Corrigan, D. A., Zimmerman, A. H., Eds.; Electrochemical Society: Pennington, NJ, 1990; Vols. 90−94, p 1.

(26) Barnard, R.; Randell, C. F.; Tye, F. L. *J. Appl. Electrochem.* **1980**, *10*, 109.

(27) Singh, D. *J. Electrochem. Soc.* **1998**, *145*, 116.

(28) Poizot, P.; Laruelle, S.; Grugeon, S.; Dupont, L.; Tarascon, J. M. *Nature* **2000**, *407*, 496.

(29) Motupally, S.; Streiz, C. C.; Weidner, W. J. *J. Electrochem. Soc.* **1998**, *145*, 29.

(30) Wang, X. Y.; Yan, J.; Zhang, Y. S.; Yuan, H. T.; Song, D. Y. *J. Appl. Electrochem.* **1998**, *28*, 1377.

(31) Penn, R. L.; Stone, A. T.; Veblen, D. R. *J. Phys. Chem. B* **2001**, *105*, 4690.

(32) Bommel, K. J. C.; Friggeri, A.; Shinkai, S. *Angew. Chem., Int. Ed.* **2003**, *42*, 980.

(33) (a) Ismail, A. F.; Dunkin, I. R.; Gallivan, S. L. *Polymer* **1999**, *40*, 6499. (b) Zhao, C. S.; Liu, X. D.; Nomizu, M.; Nishi, N. *Biomaterials* **2003**, *24*, 3747.